Prompt inclusive production of J/ψ, ψ' and χ_c mesons at the LHC in forward directions within the NRQCD k_t-factorization approach: Search for the onset of gluon saturation

Anna Cisek[1,*] and Antoni Szczurek[2,1,†]

[1]Faculty of Mathematics and Natural Sciences, University of Rzeszów, ulica Pigonia 1, PL-35-310 Rzeszów, Poland

[2]Institute of Nuclear Physics, Polish Academy of Sciences, ulica Radzikowskiego 152, PL-31-342 Kraków, Poland

(Received 29 December 2017; published 28 February 2018)

We discuss prompt production of J/ψ mesons in proton-proton collisions at the LHC within the NRQCD k_t-factorization approach using Kimber-Martin-Ryskin (KMR) unintegrated gluon distributions (UGDF). We include both direct color-singlet production ($gg \to J/\psi g$) as well as a feed down from $\chi_c \to J/\psi\gamma$ and $\psi' \to J/\psi X$ decays. The production of the decaying mesons (χ_c or ψ') is also calculated within the NRQCD k_t-factorization approach. The corresponding matrix elements for $gg \to J/\psi$ g, $gg \to \psi' g$ and $gg \to \chi_c$ include parameters of the nonrelativistic space wave functions of the quarkonia at $r = 0$, which are taken from potential models in the literature. We get the ratio of the corresponding cross section ratio for $\chi_c(2)$-to-$\chi_c(1)$ at midrapidities much closer to experimental data than obtained in a recent analysis. Differential distributions in rapidity and transverse momentum of J/ψ and ψ' are calculated and compared with experimental data of the ALICE and LHCb Collaborations. We discuss a possible onset of gluon saturation effects in the production of J/ψ and χ_c mesons at forward/backward rapidities. We show that it is necessary to modify the standard KMR UGDF to describe ALICE and LHCb data. A mixed UGDF scenario was proposed. Then, we can describe the experimental data for J/ψ production within model uncertainties with a color-singlet component only. Therefore, our theoretical results leave only relatively small room for the color-octet contributions. We discuss relations to other models in the literature. The results for the so-called hybrid model are compared to the results of the original k_t-factorization approach.

DOI: 10.1103/PhysRevD.97.034035

I. INTRODUCTION

There is a long-standing lack of convergence in understanding production of J/ψ quarkonia in proton-proton or proton-antiproton collisions. Some authors believe that the corresponding cross sections are dominated by the so-called color-octet contribution. On the other hand, some other authors expect that the color-singlet contribution dominates. The color-octet contribution cannot be calculated from first principle and is rather fitted to the experimental data. The fits lead to different sizes of the color-octet contribution, depending on the details of calculations of the color-singlet contribution(s). In many cases, successful fits were obtained, but in our opinion, there is no clear understanding of the problem. Different fits from the literature give different magnitudes of the color-octet contributions classified according to quantum numbers of the $c\bar{c}$ system.

In the present paper, we calculate the color-singlet contributions in the NRQCD k_t-factorization approach and see how much room is left for the more difficult color-octet contribution.

It is known that a sizeable part of the J/ψ production comes from radiative decays of χ_c mesons. Therefore, in the following, we have to include also this contribution very carefully trying to confront with experimental data for χ_c production whenever possible.

In a very recent k_t-factorization analysis of χ_c production [1], the authors found very different values of the nonrelativistic wave function at the origin for $\chi_c(1)$ and $\chi_c(2)$,

$$|R'_{\chi_c(1)}(0)|^2 \approx 5|R'_{\chi_c(2)}(0)|^2, \tag{1.1}$$

from a fit based on the k_t-factorization approach to LHC data. This large modification would put in doubt either the NRQCD approach and/or validity of the leading-order k_t-factorization. In the standard potential model, one obtains the same radial wave function for different χ_c

*acisek@ur.edu.pl
†antoni.szczurek@ifj.edu.pl

species [2]. Here, we diccuss also this element of the whole construction. In the following, we use Kniehl-Vasin-Saleev matrix elements which are given explicitly in Ref. [3].

Finally, the ψ' quarkonium also has a sizeable branching fraction into $J/\psi X$ [4]. Fortunately, this contribution is much smaller than the direct one as is discussed in this paper. It was considered recently in almost identical approach in [5].

In the present approach, we concentrate rather on small transverse momenta of J/ψ or ψ' relevant for ALICE and LHCb data [6–10]. We expect that color-singlet contributions may dominate in this region of the phase space.

II. SOME THEORETICAL ASPECTS

In the following, we consider only color-singlet mechanisms and look at how much room is left for color-octet production.

A. Main contributions

The main color-singlet mechanism of the J/ψ meson production is illustrated in Fig. 1. In this case, J/ψ is produced in association with an extra "hard" gluon due to C-parity conservation.

We calculate the dominant color-singlet $gg \to J/\psi g$ contribution taking into account transverse momenta of initial gluons. In the k_t-factorization approach, the differential cross section can be written as

$$\begin{aligned}\frac{d\sigma(pp \to J/\psi g X)}{dy_{J/\psi} dy_g d^2p_{J/\psi,t} d^2p_{g,t}} &= \frac{1}{16\pi^2 \hat{s}^2} \int \frac{d^2q_{1t}}{\pi}\frac{d^2q_{2t}}{\pi} \overline{|\mathcal{M}^{\text{off-shell}}_{g^*g^*\to J/\psi g}|^2} \\ &\times \delta^2(\vec{q}_{1t} + \vec{q}_{2t} - \vec{p}_{H,t} - \vec{p}_{g,t}) \\ &\times \mathcal{F}_g(x_1, q_{1t}^2, \mu^2)\mathcal{F}_g(x_2, q_{2t}^2, \mu^2), \end{aligned} \tag{2.1}$$

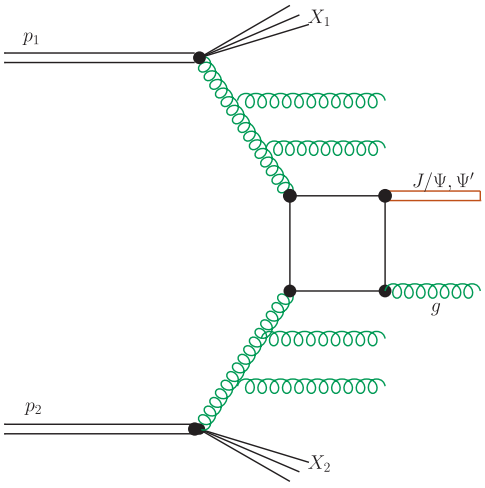

FIG. 1. Leading-order diagram for direct J/ψ (ψ') meson production in the k_t-factorization approach.

where $\mathcal{F}_g$ are unintegrated (or transverse-momentum-dependent) gluon distributions. The matrix elements were calculated as was explained, for example, in [11,12]. The corresponding matrix element squared for the $gg \to J/\psi g$ is

$$|\mathcal{M}_{gg\to J/\psi g}|^2 \propto \alpha_s^3 |R(0)|^2. \tag{2.2}$$

Running coupling constants are used in the present calculation. Different combinations of renormalization scales were tried. We decided to use

$$\alpha_s^3 \to \alpha_s(\mu_1^2)\alpha_s(\mu_2^2)\alpha_s(\mu_3^2), \tag{2.3}$$

where $\mu_1^2 = q_{1t}^2$, $\mu_2^2 = q_{2t}^2$ and $\mu_3^2 = m_t^2$ (prescription 1) or $\mu_1^2 = \max(q_{1t}^2, m_t^2)$, $\mu_2^2 = \max(q_{2t}^2, m_t^2)$ and $\mu_3^2 = m_t^2$ (prescription 2), where here m_t is the J/ψ transverse mass. The factorization scale in the calculation was taken as $\mu_F^2 = (m_t^2 + p_{t,g}^2)/2$.

Similarly, we do calculations for the P-wave χ_c meson production. Here, the lowest-order subprocess $gg \to \chi_c$ is allowed by positive C-parity of χ_c mesons. In the k_t-factorization approach, the leading-order cross section for the χ_c meson production can be written somewhat formally as

$$\begin{aligned}\sigma_{pp\to\chi_c} = \int &\frac{dx_1}{x_1}\frac{dx_2}{x_2}\frac{d^2q_{1t}}{\pi}\frac{d^2q_{2t}}{\pi} \\ &\times \delta((q_1+q_2)^2 - M_{\chi_c}^2)\sigma_{gg\to H}(x_1,x_2,q_1,q_2) \\ &\times \mathcal{F}_g(x_1, q_{1t}^2, \mu_F^2)\mathcal{F}_g(x_2, q_{2t}^2, \mu_F^2), \end{aligned} \tag{2.4}$$

where $\mathcal{F}_g$ are unintegrated (or transverse-momentum-dependent) gluon distributions and $\sigma_{gg\to\chi_c}$ are $gg \to \chi_c$ (off-shell) cross sections. The situation is illustrated diagramatically in Fig. 2.

The matrix element squared for the $gg \to \chi_c$ subprocess is

$$|\mathcal{M}_{gg\to\chi_c}|^2 \propto \alpha_s^2 |R'(0)|^2. \tag{2.5}$$

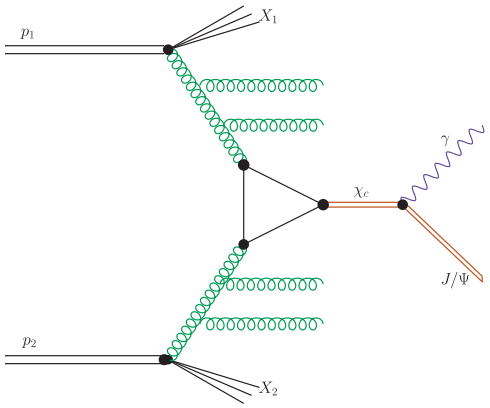

FIG. 2. Leading-order diagram for χ_c meson production in the k_t-factorization approach.

After some manipulation,

$$\sigma_{pp\to\chi_c} = \int dy d^2p_t d^2q_t \frac{1}{sx_1x_2}\frac{1}{m^2_{t,\chi_c}} \times \overline{|\mathcal{M}_{g^*g^*\to\chi_c}|^2}\mathcal{F}_g(x_1,q^2_{1t},\mu^2_F) \times \mathcal{F}_g(x_2,q^2_{2t},\mu^2_F)/4, \quad (2.6)$$

that can be also used to calculate rapidity and transverse momentum distribution of the χ_c mesons.

In the last equation, $\vec{p}_t = \vec{q}_{1t} + \vec{q}_{2t}$ is the transverse momentum of the χ_c meson and $\vec{q}_t = \vec{q}_{1t} - \vec{q}_{2t}$ is the auxiliary variable which is used for the integration of the cross section. Furthermore, m_{t,χ_c} is the so-called χ_c transverse mass and $x_1 = \frac{m_{t,\chi_c}}{\sqrt{s}}\exp(y)$, $x_2 = \frac{m_{t,\chi_c}}{\sqrt{s}}\exp(-y)$. The factor $\frac{1}{4}$ is the Jacobian of transformation from $(\vec{q}_{1t},\vec{q}_{2t})$ to $(\vec{p}_t,\vec{q}_t)$ variables.

As for the J/ψ production, running coupling constants are used. Different combination of scales were tried. The best choices are

$$\alpha_s^2 \to \alpha_s(\mu_1^2)\alpha_s(\mu_2^2), \quad (2.7)$$

where $\mu_1^2 = q_{1t}^2$ and $\mu_2^2 = q_{2t}^2$ (prescription 1) or $\mu_1^2 = \max(q_{1t}^2, m_t^2)$ and $\mu_2^2 = \max(q_{2t}^2, m_t^2)$ (prescription2). Above, m_t is the transverse mass of the χ_c meson.

The factorization scale(s) for the χ_c meson production are fixed traditionally as $\mu_F^2 = m_t^2$.

The J/ψ mesons are produced then by the $\chi_c \to J/\psi\gamma$ decays which are dominated by E1 transitions [13,14]. This channel cannot be easily eliminated experimentally as the produced photons are usually rather soft. Due to the same reasons, χ_c mesons can be measured at large transverse momenta or very forward/backward directions.

B. Unintegrated gluon distributions

In the present analysis, the Kimber-Martin-Ryskin KMR UGDFs [15] are used, which are generated from conventional collinear MMTH2014LO PDFs [16]. In actual calculations of distributions, we interpolate them on a three-dimensional grid in $\log_{10}(x)$, $\log_{10}(k_t^2)$ and $\log_{10}(\mu^2)$ prepared before the calculation of the production cross section or differential distributions.

The KMR UGDF was succesfully used, for example, for production of charm and charmed mesons [17,18] as well as for production of two pairs of $c\bar{c}$ [19,20].

In a standard approach, the KMR UGDFs are calculated for larger values of gluon transverse momenta and are usually frozen at small gluon transverse momenta. The value at which the freezing is applied is independent of all other variables, longitudinal momentum fraction, in particular. The UGDFs used in calculations neglect possible effects of saturation. For small initial gluon momenta, $k_{1t}^2 < Q_s^2$ or $k_{2t}^2 < Q_s^2$, and for forward/backward production, some effects of gluon saturation may be expected. The saturation scale as is often parametrized as

$$Q_s^2(x) = Q_0^2(x_0/x)^\lambda. \quad (2.8)$$

One could correct the original KMR distributions by assuming saturation of UGDFs for $k_{it}^2 < Q_s^2$,

$$\mathcal{F}_A(x,k_t^2,\mu^2) = \text{const for } k_t^2 < Q_s^2. \quad (2.9)$$

We call this model of UGDF "saturation A" for brevity. For comparison, we consider also faster damping of the small-k_t region by multiplying the $\mathcal{F}_A$ by an extra damping factor,

$$\mathcal{F}_B(x,k_t^2,\mu^2) = (k_t^2/Q_s^2)\mathcal{F}_A(x,k_t^2,\mu^2). \quad (2.10)$$

We call this model of UGDF "saturation B" for brevity. Another, called "mixed UGDF", scenario is discussed in the text. Some consequences of the small-k_t corrections are discussed in the following section.

III. RESULTS

A. ψ' production

We start with ψ' production. In Fig. 3, we show rapidity distributions of ψ' obtained with the KMR unintegrated

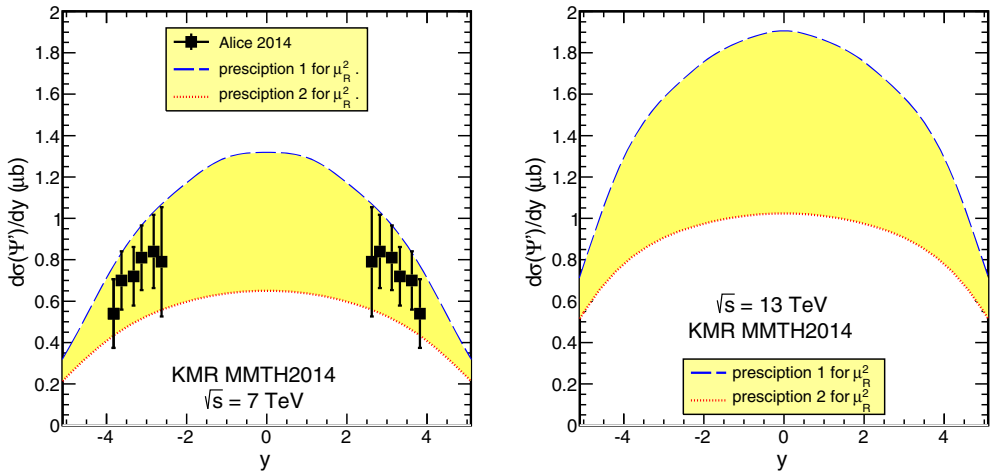

FIG. 3. Rapidity distribution of ψ' meson (direct mechanism) for the KMR UGDF for $\sqrt{s} = 7$ TeV (left panel) and $\sqrt{s} = 13$ TeV (right panel). The upper line is for the scale prescription 1, and the lower line is for prescription 2.

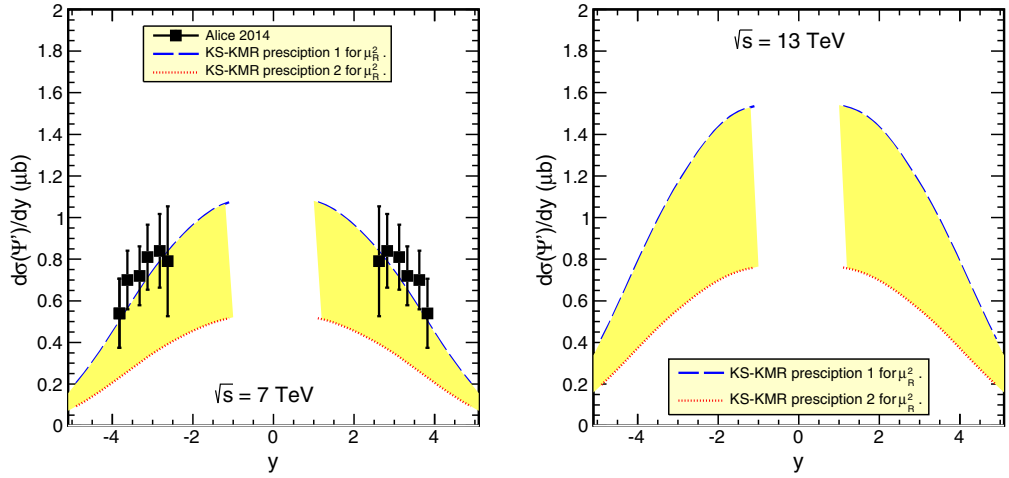

FIG. 4. Rapidity distribution of ψ' meson (direct mechanism) for the mixed UGDFs for $\sqrt{s} = 7$ TeV (left panel) and $\sqrt{s} = 13$ TeV (right panel). The upper line is for scale prescription 1, and the lower line is for prescription 2.

gluon distributions. In the left panel, we compare our results with the ALICE experimental data for $\sqrt{s} = 7$ TeV [8]. The ALICE Collaboration measured only ψ' mesons emitted in rather forward directions. This corresponds to one longitudinal momentum fraction small and the second longitudinal momentum fraction large. We show results with the two different prescriptions for the arguments of the QCD running coupling constant as was discussed in the previous section. One gets a rather large uncertainty band associated with the choice of the α_s argument. On the right panel, we show our predictions for $\sqrt{s} = 13$ TeV.

For very small x, one may expect saturation effects. The KMR UGDF does not include such effects. To illustrate the potential effect instead of using both UGDFs of the same type (KMR) for large x_1/x_2, we take the KMR UGDF, whereas for small x_2/x_1, we take, for example, the Kutak-Stasto nonlinear UGDF [21]. It is marked by the KS acronym in Fig. 4. A slightly smaller cross section has been obtained than with the KMR UGDF. The effect is, however, not significant.

Since the ψ' meson decays $\psi' \to J/\psi X$ with BF = 0.61 [4], it constitutes also a contribution to the J/ψ channel and is taken into account in the rest of the paper.

B. J/Ψ direct production

There are three components of prompt J/ψ production: direct production (see Figs. 5–8) and feed down from ψ' and χ_c decays.

In this subsection, we present results for the direct component for J/ψ production. In Fig. 5, we show exclusively this contribution for three different collision energies: $\sqrt{s} = 2.76$ TeV (left panel), $\sqrt{s} = 7$ TeV (middle panel) and $\sqrt{s} = 13$ TeV (right panel). As for ψ' production, we show our results for two different prescriptions for α_s and for the KMR UGDF. As for the ψ' production, there is large uncertainty related to the choice of running coupling constant (see the yellow band). The direct contribution is large, but there is a room for other contributions, which are discussed in the following.

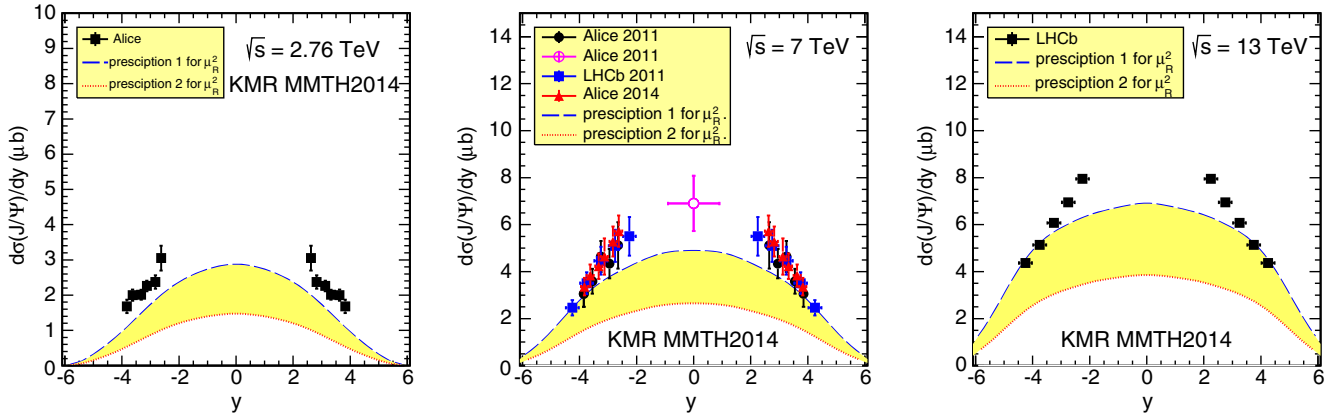

FIG. 5. Rapidity distribution of J/ψ mesons (direct mechanism) for the KMR UGDF for $\sqrt{s} = 2.76$ TeV (left panel), $\sqrt{s} = 7$ TeV (middle panel) and $\sqrt{s} = 13$ TeV (right panel). The upper line is for the scale prescription 1, and the lower line is for prescription 2. The results are compared with the ALICE [6–8] and LHCb [9,10] experimental data.

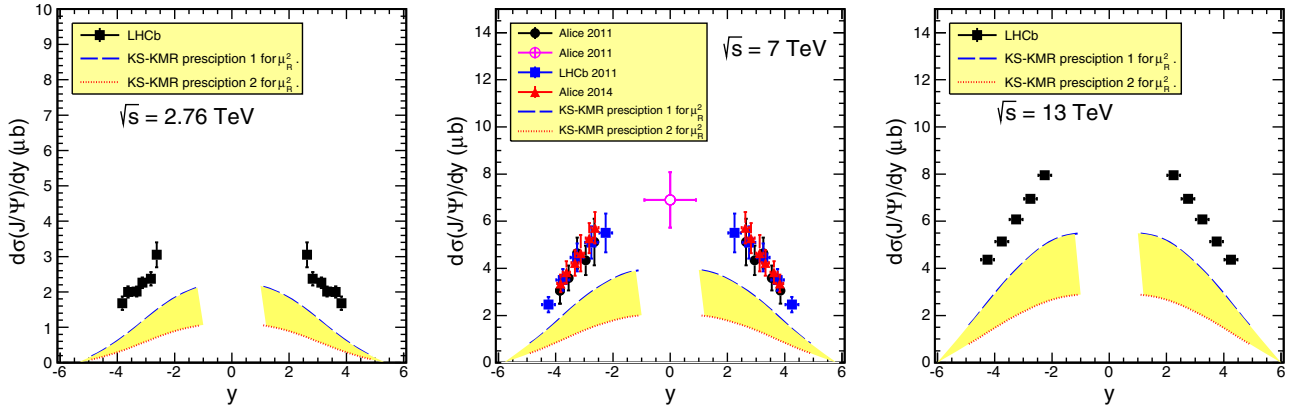

FIG. 6. Rapidity distribution of J/ψ mesons (direct mechanism) for the mixed UGDFs for $\sqrt{s} = 2.76$ GeV (left panel), $\sqrt{s} = 7$ TeV (middle panel) and $\sqrt{s} = 13$ TeV (right panel). The upper line is for the scale prescription 1, and the lower line is for prescription 2.

For completeness in Fig. 6, we show also our results with the mixed UGDFs scenario described above. Here, the effect of UGDF modification is similar as for ψ'.

We look also for transverse momentum distributions. For example, the LHCb Collaboration measured such distributions for different intervals of rapidity [9,10]. In Fig. 7, we show such distributions for $\sqrt{s} = 7$ TeV for

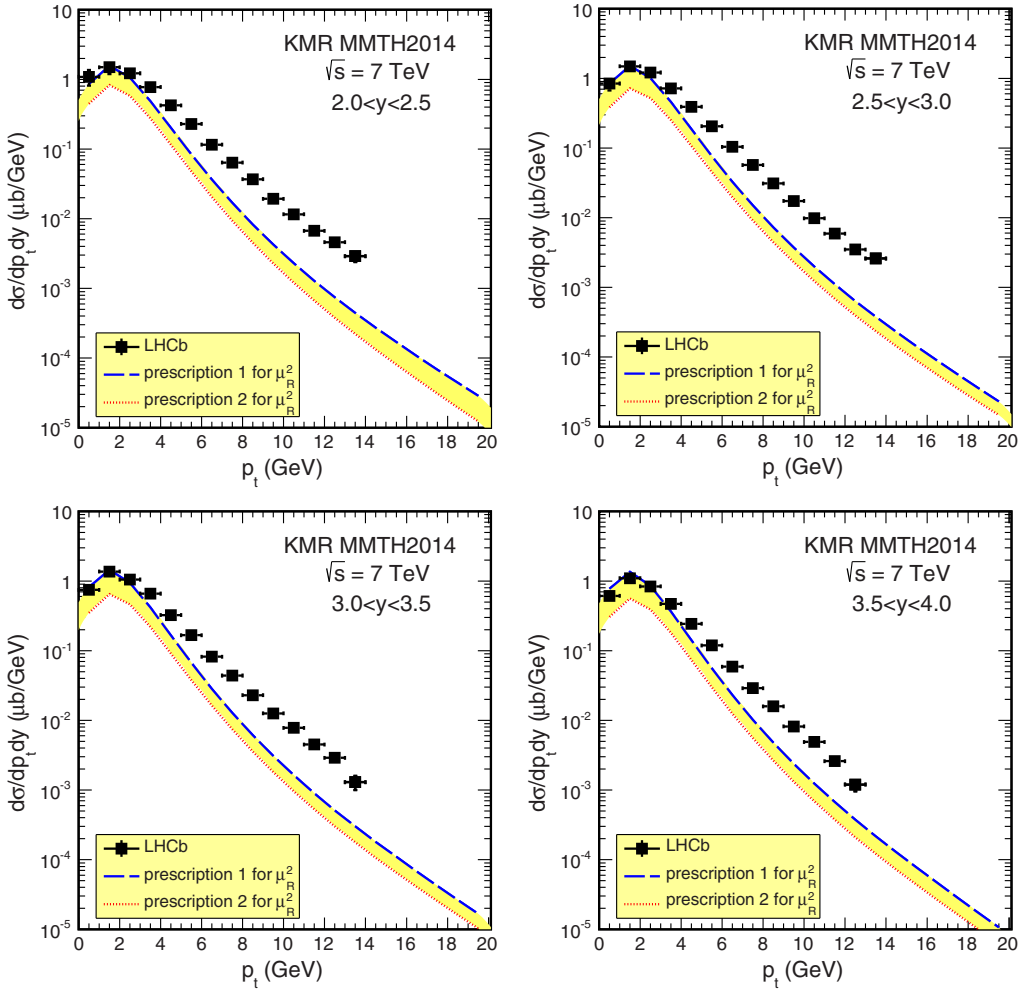

FIG. 7. Transverse momentum distribution of J/ψ (direct component only) together with LHCb [9] experimental data for $\sqrt{s} = 7$ TeV for different ranges of rapidity specified in the figures.

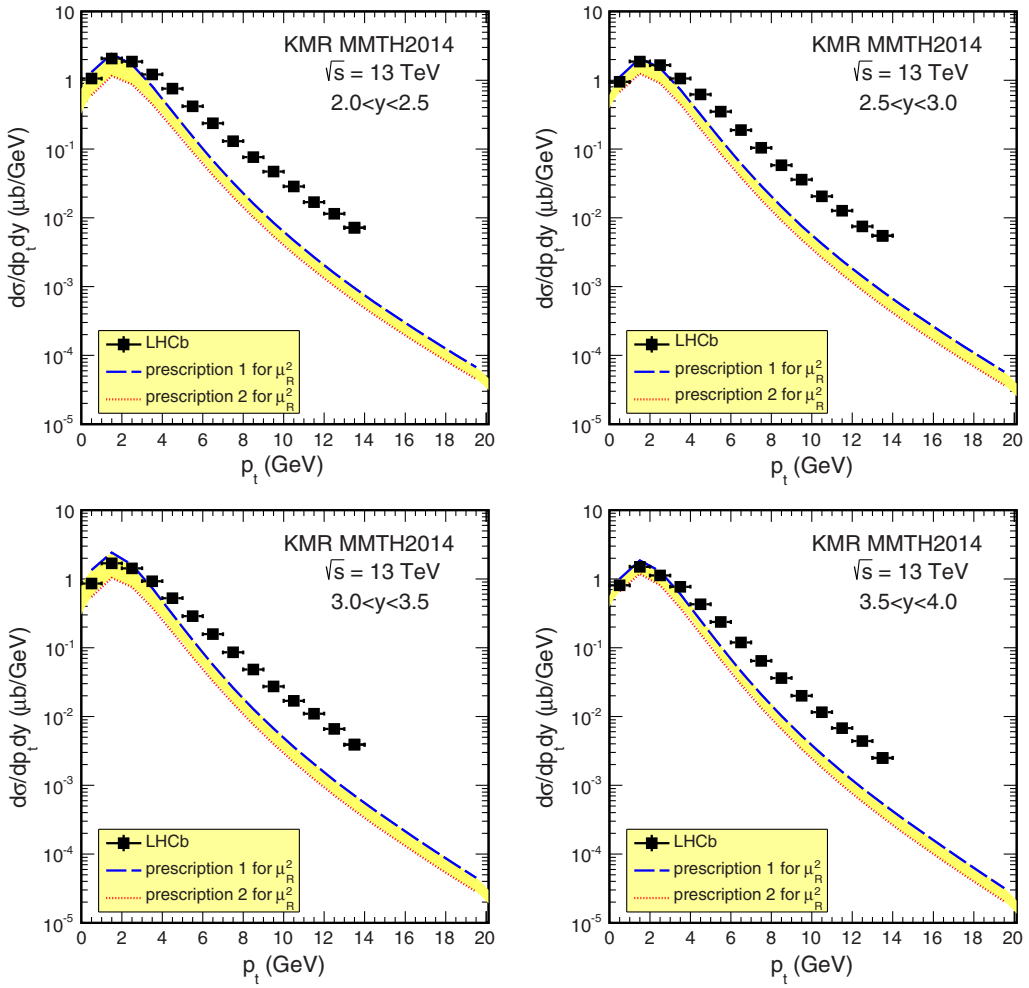

FIG. 8. Transverse momentum distribution of J/ψ (direct component only) together with LHCb [10] experimental data for $\sqrt{s} = 13$ TeV for different ranges of rapidity specified in the figures.

two different prescriptions of α_s. Our direct component exhausts a large fraction of the cross section for small p_t. At larger p_t, clearly some other contributions are missing.

In Fig. 8, we show similar distributions for $\sqrt{s} = 13$ TeV. The situation is very much the same as for $\sqrt{s} = 7$ TeV.

C. J/ψ from χ_c decays

Now we proceed to the important contribution of J/ψ originating from the feed down from the χ_c production and decay. The $\chi_c(0)$ meson has a very small branching fraction for decay $\chi_c(0) \to J/\psi\gamma$ (BR $= 0.0127$ [4]). Therefore, in the following, we take into account only production and decays of $\chi_c(1)$ (BF $= 0.339$ [4]) and $\chi_c(2)$ (BF $= 0.192$ [4]). In Fig. 9, we show rapidity distributions of resulting J/ψ mesons for two different prescriptions of α_s (compare top and bottom panels) for three different energies $\sqrt{s} = 2.76$, 7, 13 TeV. This calculations were performed with the KMR UGDF. For comparison, we present also existing data of the ALICE and LHCb Collaborations. We show both contributions of each of the mesons and a sum of them. The first prescription leads to a clearly too large cross section, having in mind the other missing contributions. This is especially clearly seen for $\sqrt{s} = 13$ TeV, at large rapidities. The second prescription is not in conflict with the data, but one should remember other, not yet included, contributions (direct one and ψ' feed down).

The situation with χ_c production seems more problematic than for the direct contribution and not yet discussed ψ' feed down. What is specific for χ_c production? In Fig. 10, we show averaged values of x_1 and x_2 being arguments of UGDFs. Clearly, in the forward LHCb rapidity region, the corresponding longitudinal momentum fractions are extremely small. For $\sqrt{s} = 13$ TeV, they reach the gluon longitudinal momentum fractions as small as $x \sim 10^{-6}$. This makes the forward production of χ_c very special in the context

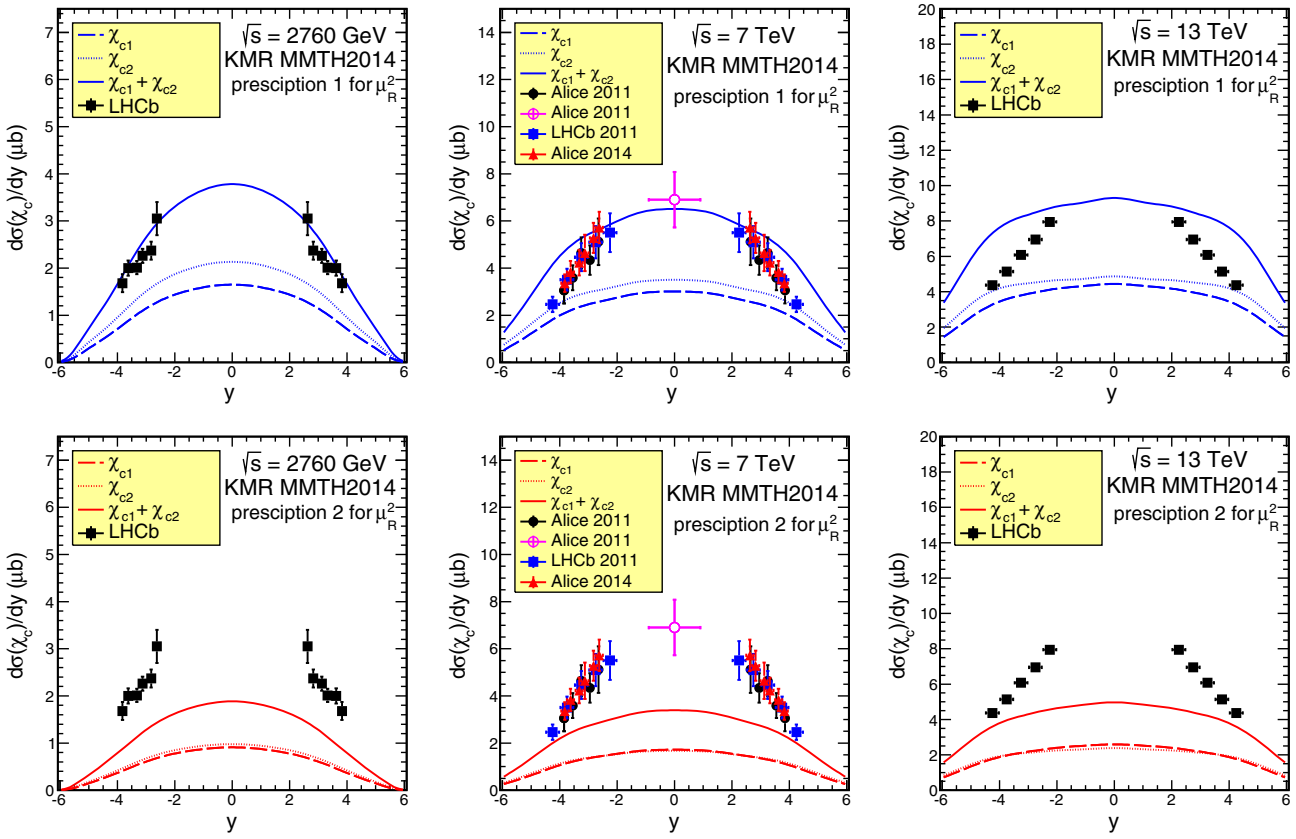

FIG. 9. Rapidity distribution of J/ψ mesons (from χ_c decays) for the KMR UGDF for $\sqrt{s} = 2.76$ GeV (left panel), $\sqrt{s} = 7$ TeV (middle panel) and $\sqrt{s} = 13$ TeV (right panel). The upper plots are for the scale prescription 1, and the lower plots are for prescription 2.

of searching for saturation/nonlinear effects. We show results when the averaging is performed in different regions of χ_c transverse momenta.

The very small values of longitudinal momentum fractions relevant for χ_c production in the forward directions fully justify the use of the "mixed" UGDFs, discussed already in the context of direct production. In Fig. 11, we show corresponding rapidity distributions. The results obtained for the "mixed" distributions are quite different than those obtained solely with the KMR UGDFs, especially for $\sqrt{s} = 13$ TeV. Is it a sign of the onset of saturation? This should be clarified in the future by dedicated measurements of χ_c mesons for different rapidities. This process seems to be very promising in this context.

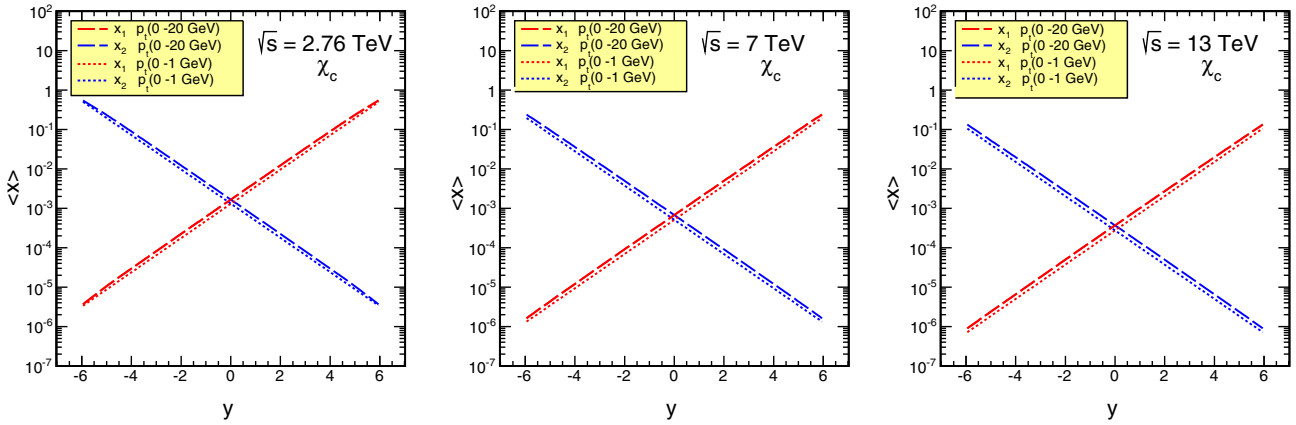

FIG. 10. Average longitudinal momentum fractions x_1 and x_2 as a function of y (rapidity of χ_c) for different ranges of χ_c transverse momenta as specified in the figures.

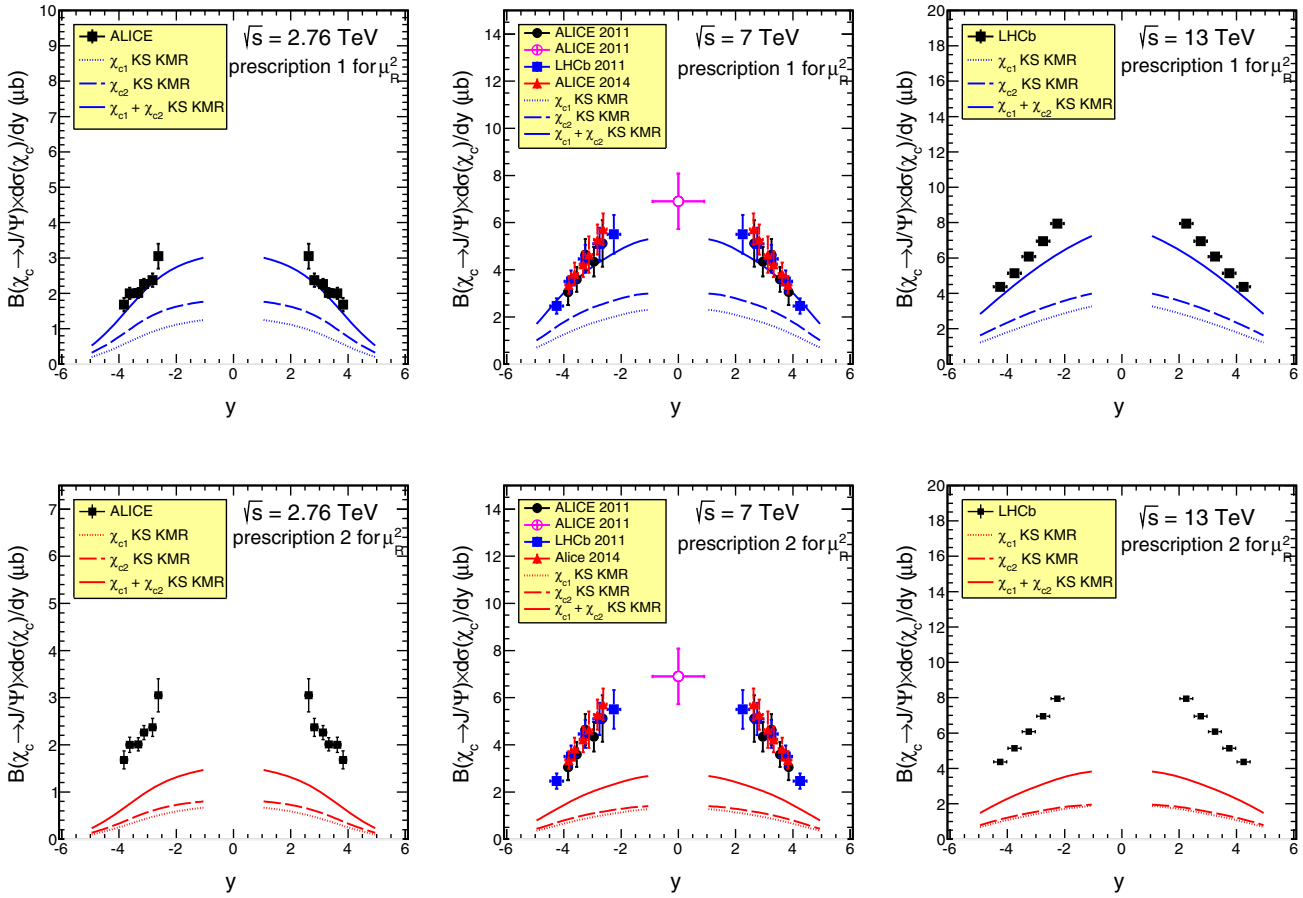

FIG. 11. Rapidity distribution of J/ψ mesons (from χ_c decays) for the mixed UGDFs for $\sqrt{s} = 2.76$ GeV (left panel), $\sqrt{s} = 7$ TeV (middle panel) and $\sqrt{s} = 13$ TeV (right panel). The upper plots are for the scale prescription 1, and the lower plots are for prescription 2.

D. χ_c production

So far χ_c mesons were measured only at $\sqrt{s} = 7$ TeV, at midrapidities and rather large transverse momenta. Then, the corresponding longitudinal momentum fractions are not so small. In Fig. 12, we show our results for both $\sqrt{s} = 7$ TeV, together with ATLAS experimental data [22], and our predictions for $\sqrt{s} = 13$ TeV. We get a reasonable, but not ideal, description of the experimental transverse momentum distributions for $\chi_c(1)$ (left panel) and $\chi_c(2)$ (middle panel). We slightly overestimate the data for $\chi_c(2)$ especially for smaller values of transverse momenta. For completeness, we show the ratio $\chi_c(2)/\chi_c(1)$. In principle, we could try to treat parameters of $\chi_c(1)$ and $\chi_c(2)$ independently and better fit them to the ATLAS data, but we leave it for the future when next-to-leading order corrections will be included. Summarizing this short subsection, we have shown that our parameters for χ_c are reasonable. They are to some extent effective as only leading-order k_t-factorization is done here. How it changes at next-to-leading order clearly goes beyond the scope of the present analysis.

E. All contributions for J/ψ production

Having reviewed all components separately, we are ready to include all of them together. In the following, we adopt always prescription 2 (lower limits above) for α_s as an example.

In Fig. 13, we show corresponding results for the KMR UGDF. While we get a good description of the experimental distribution for $\sqrt{s} = 2.76$ TeV, it is slightly worse for $\sqrt{s} = 7$ TeV and clear disagreement for $\sqrt{s} = 13$ TeV. The disagreement is larger for larger rapidities (smaller longitudinal momentum fractions). This may be related to onset of saturation in this region of phase space and is worthy of further study.

In Fig. 14, we show similar results for the "mixed" scenario. We get too much damping of the cross section, especially for largest $\sqrt{s}$. This may signal also the presence of other, nonincluded, mechanisms or may signal that the KS saturation effects are too strong. They may also appear too early in x.

Since, as discussed above, the longitudinal momentum fractions for J/ψ and ψ' are about an order of magnitude larger than those for χ_c production, we consider also a new scenario. Here, we take standard KMR UGDFs for the S-wave quarkonia and "mixed" UGDFs for the χ_c mesons. The resulting distributions are shown in Fig. 15. The agreement with the experimental data is very good, but we cannot draw too strong conclusions. More systematic

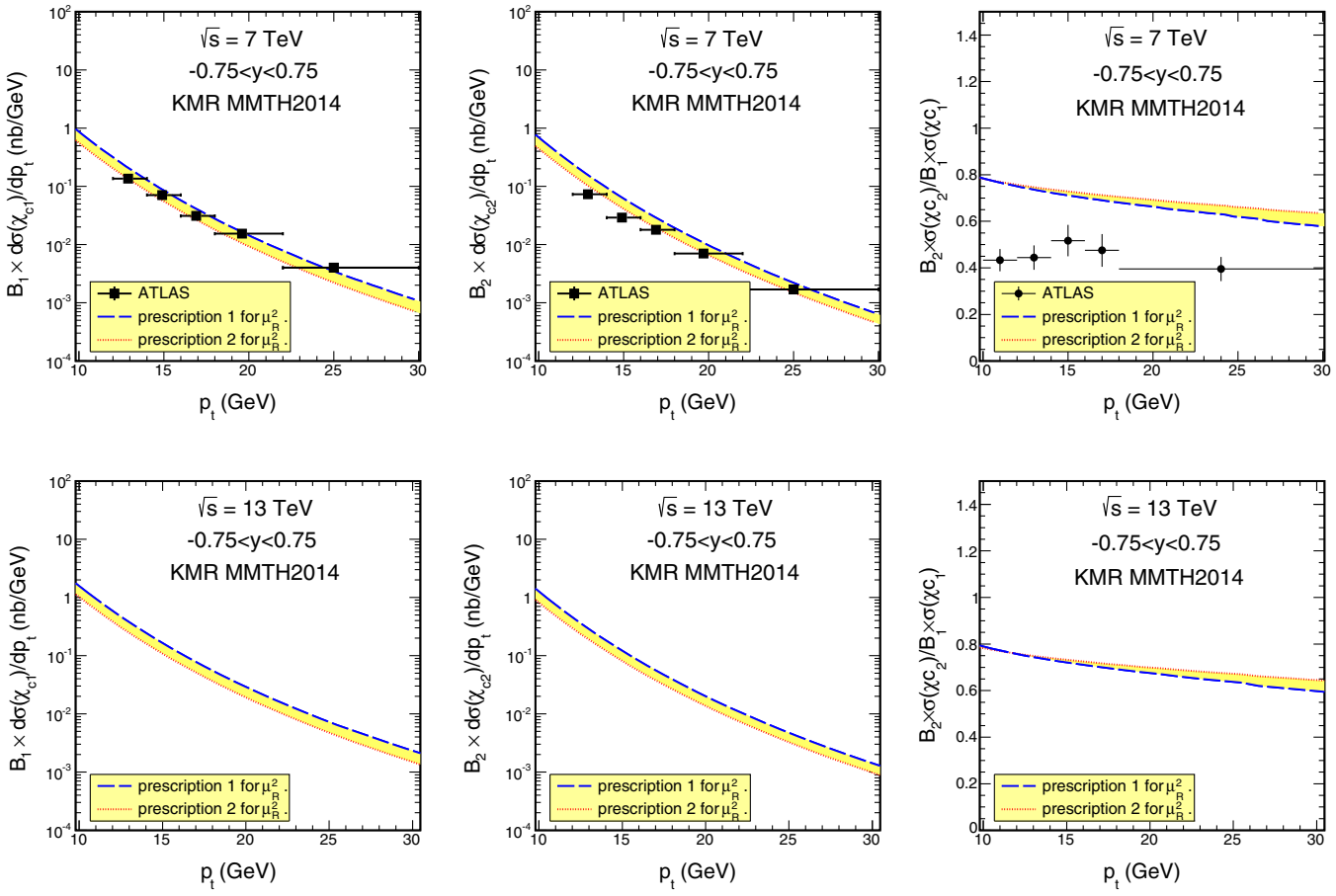

FIG. 12. Transverse momentum distributions of $\chi_c(1)$ (left panels) and $\chi_c(2)$ (middle panels). The right panels show the ratio of $\chi_c(2)$ to $\chi_c(1)$. The upper plots are for $\sqrt{s} = 7$ TeV, and the lower plots are for $\sqrt{s} = 13$ TeV. The experimental ATLAS [22] data are shown for comparison.

studies of low-p_t distributions of J/ψ and χ_c mesons would certainly be very useful in this context.

F. General comments and relations to other approaches in the literature

In very forward directions, often a so-called hybrid approach is applied for different reactions, like forward jet or dijet production. In this approach, one uses one collinear parton distribution and one unintegrated gluon distribution. The hybrid model is claimed to be a sensible approximation in very forward directions [large x_F of the produced object(s)], when one of the longitudinal fractions (x_1 or x_2) is very small and the second longitudinal fraction is large. At the LHCb or forward ALICE measurements for

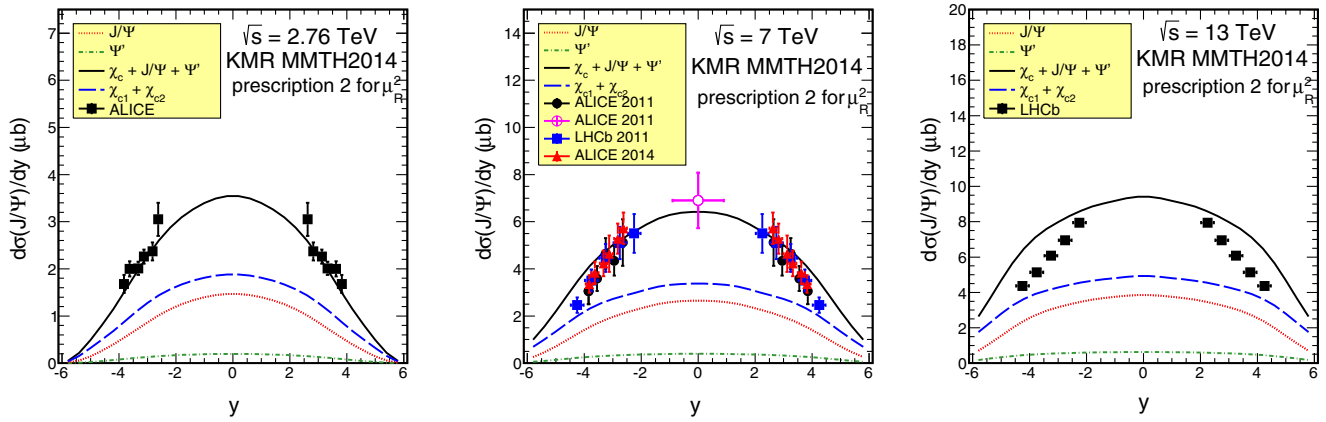

FIG. 13. Rapidity distribution of J/ψ mesons for all considered mechanisms for three different energies. In this calculation, for all cases, the KMR UGDF and prescription 2 were used.

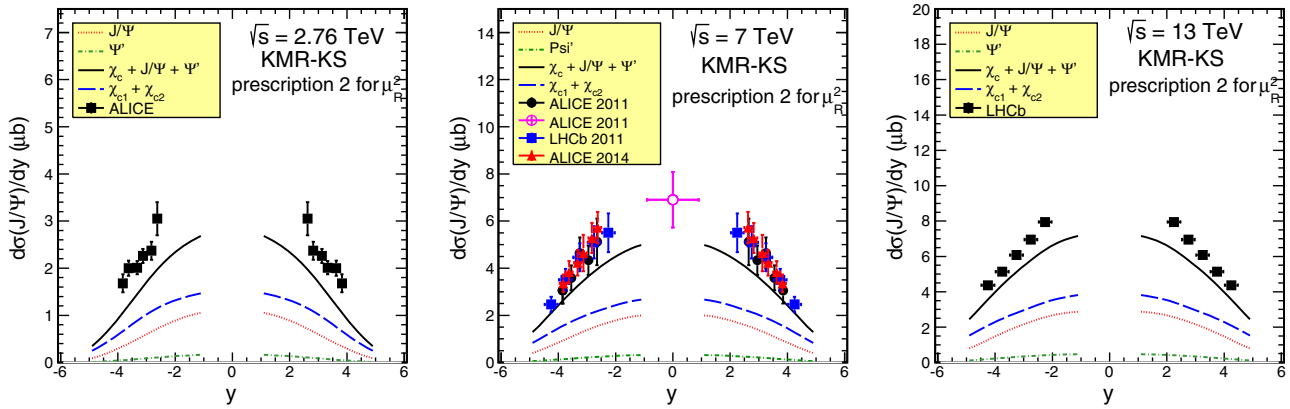

FIG. 14. Rapidity distribution of J/ψ mesons for all considered mechanisms for three different energies. In this calculation, for all cases (J/ψ, ψ' and χ_c), the mixed UGDFs scenario and prescription 2 were used.

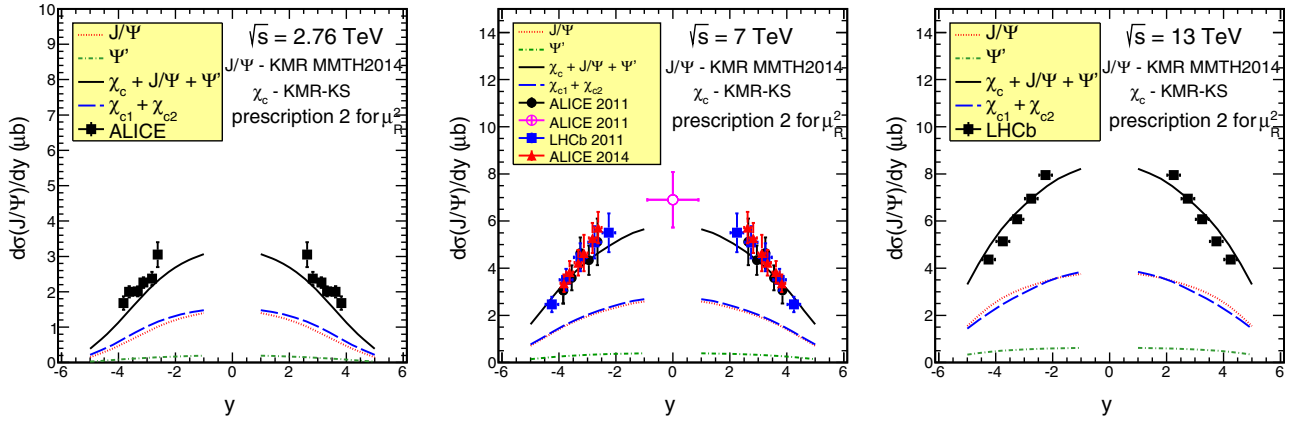

FIG. 15. Rapidity distribution of J/ψ mesons for all considered mechanisms for three different energies. In this calculation, only for χ_c production, the mixed UGDFs scenario was used.

the high collision energies $\sqrt{s} = 7$, 8, 13 TeV and relatively small transverse momenta of χ_c or J/ψ, both x's are rather small x_1, $x_2 < 10^{-1}$ (see Fig. 10). For the LHCb rapidity coverage, $x_F < 0.05$. Therefore, for the high energy collisions and so-called "forward" LHCb rapidity region, this is still a rather "central" rapidity region in the sense of the longitudinal momentum fractions. The corresponding larger gluon longitudinal fractions ($\max\{x_1, x_2\}$) are similar as those for central rapidities at RHIC.

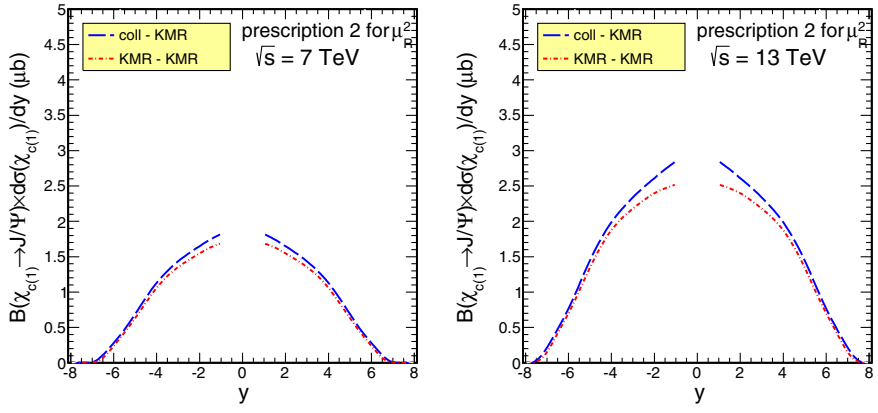

FIG. 16. Rapidity distribution of $\chi_c(1)$ meson in the hybrid model and compared to the k_t-factorization approach. The left panel is for $\sqrt{s} = 7$ TeV, and the right panel is for $\sqrt{s} = 13$ TeV.

We showed in our previous works that the inclusive D meson production at the LHCb can be described nicely within the original k_t-factorization, see, e.g., [19]. We checked that the hybrid approach is not the best there and leads to a deficit of the cross section for $\sqrt{s} = 7$ and 8 TeV. Now, we show some results of the hybrid model and a comparison to the results obtained within the original k_t-factorization approach. In Fig. 16, for example, we show rapidity distribution of $\chi_c(1)$ mesons ($2 \to 1$ partonic process). The hybrid model gives almost the same result as the original k_t-factorization approach. In Fig. 17, we show corresponding transverse momentum distribution obtained by integrating over the LHCb rapidity region $2.0 < y < 4.5$. Also, here, the agreement is quite good.

Finally, in Fig. 18, we show rapidity distribution for a directly produced J/ψ meson (the $gg \to J/\psi g$ $2 \to 2$ partonic process). Here, the agreement between the two approaches is not so good. This may be partially understood by the fact that forward J/ψ does not automatically mean also forward gluon. The situation here is similar as for open charm production.

In the present study, we have focused on application of the k_t-factorization approach. There are other models in the literature. One of them is the next-to-leading order collinear approach (see, e.g., [23] and references therein). This approach is similar to our approach.

Another alternative approach is the color-evaporation model [24,25]. The old color-evaporation model has been corrected recently [26] and is also able to describe experimental data on inclusive quarkonium production, approximately even some polarization variables [27]. This approach is based, however, on a very different philosophy compared to our approach. We include only color-singlet terms with essentially no free parameters and include all known feed down contributions. As written already in our abstract, we do not see significant room for color-octet terms. So far, we have not seen studies of the improved color-evaporation model for rapidity distributions in forward region. Certainly, such an analysis would be interesting and worthy to do, but it clearly goes beyond the scope of the present approach where we focus on quite a different

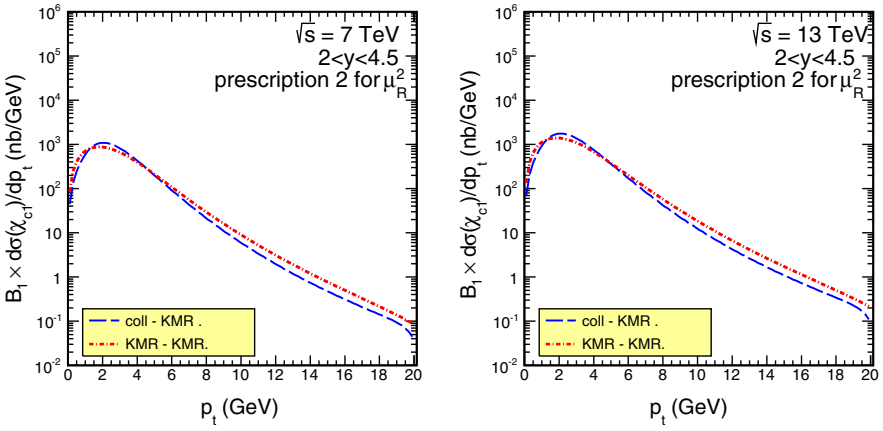

FIG. 17. Transverse momentum distribution of $\chi_c(1)$ meson in the hybrid model compared to the k_t-factorization approach for the LHCb rapidity coverage. The left panel is for $\sqrt{s} = 7$ TeV, and the right panel is for $\sqrt{s} = 13$ TeV.

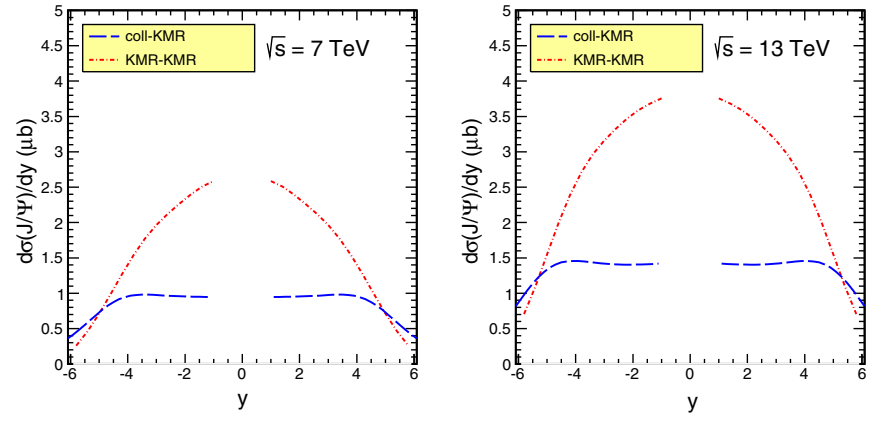

FIG. 18. Rapidity distribution of J/ψ meson produced in the direct process in the hybrid model and compared to the k_t-factorization approach with KMR UGDF. The left panel is for $\sqrt{s} = 7$ TeV, and the right panel is for $\sqrt{s} = 13$ TeV.

approach. Compared to the color-evaporation model, there are essentially no free parameters in our approach.

IV. CONCLUSIONS

In the present paper, we have focused on the calculation of cross sections for inclusive prompt production of J/ψ and ψ' in forward directions within the k_t-factorization approach. In this calculation, NR QCD matrix elements were used with parameters of quarkonia $c\bar{c}$ wave functions at the origin taken from potential model(s).

In the present calculation, we have used two different sets of unintegrated gluon distribution functions: the Kimber-Martin-Ryskin UGDF based on DGLAP collinear gluon distribution function and the Kutak-Staśto UGDF which includes nonlinear effects at small x values and describes exclusive production of J/ψ [28].

We have included both the direct component and the component related to radiative decays of χ_c mesons. In general, they give similar contributions for the integrated cross section.

We have compared our results with the recent results of the ALICE and LHCb Collaborations (small transverse momenta and forward directions) at $\sqrt{s} = 7$ TeV. We have found that using standard KMR UGDF we overestimate the forward production of J/ψ in this case. The biggest contribution is given by radiative decays of χ_c mesons. We have proposed how to modify UGDFs to include possible onset of saturation effects. In this mixed UGDF scenario, a reasonable description of the data is possible. We have found that within model uncertainties (UGDFs, renormalization scale, parameters of the nonrelativistic wave function) we can almost describe the production of J/ψ or ψ' at low transverse momenta and forward direction including only color-singlet contribution.

We have discussed theoretical uncertainties related to the choice of renormalization scales. In addition, we have discussed some open issues related to the KMR UGDFs. We have shown how to modify the KMR UGDFs to include possible saturation effects. A possible onset of saturation or, in general, nonlinear effects for UGDFs was discussed, especially in the context of the LHCb data. We have found that production of χ_c mesons in forward directions is a very good way to search for the onset of saturation, because, as discussed in our paper, it probes smaller values of longitudinal momentum fraction than the J/ψ production and is therefore better suited for that purpose. Such an analysis could be done by the LHCb Collaboration.

We have also made a comparison of our k_t-factorization results to the results of the hybrid model where one collinear and one unintegrated gluon are used. This latter approach is used, for example, for forward jet production. We have found that the two approaches (hybrid and k_t-factorization) have given very similar results for χ_c production ($gg \to \chi_c$) and a bit different results for direct $gg \to J/\psi g$ production. A short explanation is given in the main text.

Other approaches have been briefly discussed, but a comparison of results goes beyond the scope of the present studies.

ACKNOWLEDGMENTS

We are indebted to Sergey Baranov, Roman Pasechnik, Vladimir Saleev and Wolfgang Schäfer for exchange of useful information. This work was partially supported by the Polish Grant No. DEC-2014/15/B/ST2/02528 (OPUS) as well as by the Centre for Innovation and Transfer of Natural Sciences and Engineering Knowledge in Rzeszów.

[1] S. P. Baranov, A. V. Lipatov, and N. P. Zotov, Phys. Rev. D **93**, 094012 (2016).
[2] E. J. Eichten and Ch. Quigg, Phys. Rev. D **52**, 1726 (1995).
[3] B. A. Kniehl, D. V. Vasin, and V. A. Saleev, Phys. Rev. D **73**, 074022 (2006).
[4] C. Patrignani *et al.* (PDG Collaboration), Chin. Phys. C **40**, 100001 (2016).
[5] S. P. Baranov, A. V. Lipatov, and N. P. Zotov, Eur. Phys. J. C **75**, 455 (2015).
[6] B. Abelev *et al.* (ALICE Collaboration), Phys. Lett. B **718**, 295 (2012).
[7] K.Aamodt *et al.* (ALICE Collaboration), Phys. Lett. B **704**, 442 (2011).
[8] B. Abelev *et al.* (ALICE Collaboration), Eur. Phys. J. C **74**, 2974 (2014).
[9] R. Aaij *et al.* (LHCb Collaboration), Eur. Phys. J. C **71**, 1645 (2011).
[10] R. Aaij *et al.* (LHCb Collaboration), J. High Energy Phys. 10 (2015) 172.
[11] S. P. Baranov, Phys. Rev. D **66**, 114003 (2002).
[12] S. P. Baranov and A. Szczurek, Phys. Rev. D **77**, 054016 (2008).
[13] M. Ambrogiani (E835 Collaboration), Phys. Rev. D **65**, 052002 (2002).
[14] P. Cho, M. Wise, and S. Trivedi, Phys. Rev. D **51**, R2039 (1995).
[15] M. A. Kimber, A. D. Martin, and M. G. Ryskin, Phys. Rev. D **63**, 114027 (2001).
[16] L. A. Harland-Lang, A. D. Martin, P. Motylinski, and R. S. Thorne, Eur. Phys. J. C **75**, 204 (2015).
[17] R. Maciuła and A. Szczurek, Phys. Rev. D **87**, 094022 (2013).

[18] R. Maciuła, A. Szczurek, and M. Łuszczak, Phys. Rev. D **92**, 054006 (2015).
[19] R. Maciuła and A. Szczurek, Phys. Rev. D **87**, 074039 (2013).
[20] A. van Hameren, R. Maciuła, and A. Szczurek, Phys. Rev. D **89**, 094019 (2014).
[21] K. Kutak and A. M. Staśto, Eur. Phys. J. C **41**, 343 (2005).
[22] G. Aad *et al.* (ATLAS Collaboration), J. High Energy Phys. 07 (2014) 154.
[23] Y.-Q. Ma, K. Wang, and K.-T. Chao, Phys. Rev. Lett. **106**, 042002 (2011).
[24] H. Fritsch, Phys. Lett. **67B**, 217 (1977).
[25] F. Halzen, Phys. Lett. **69B**, 105 (1977).
[26] Y.-Q. Ma and R. Vogt, Phys. Rev. D **94**, 114029 (2016).
[27] V. Cheung and R. Vogt, Phys. Rev. D **96**, 054014 (2017).
[28] A. Cisek, W. Schäfer, and A. Szczurek, J. High Energy Phys. 04 (2015) 159.